



## Interfacial reaction behavior and thermodynamics between Sn–xSb alloys and Cu substrate

Rong-yue WANG<sup>1</sup>, Zhang-fu YUAN<sup>1</sup>, Hong-xin ZHAO<sup>2</sup>, Xiao YANG<sup>3</sup>, Yu-hui HAO<sup>1</sup>

1. Collaborative Innovation Center of Steel Technology,

University of Science and Technology Beijing, Beijing 100083, China;

2. Institute of Process Engineering, Chinese Academy of Sciences, Beijing 100190, China;

3. School of Engineering, Westlake University, Hangzhou 310024, China

Received 27 December 2021; accepted 12 May 2022

**Abstract:** In order to determine the effect of Sb element on the welding reliability of Sn–Sb alloy solder, the interfacial behavior of Sn–Sb alloys with different Sb contents on the Cu substrate was investigated. The evolution process of interfacial layers was explained by analyzing the microstructure and interfacial reaction thermodynamics of Sn–xSb/Cu system. The addition of Sb has a non-monotonic effect on the intermetallic compound layers. Sb can inhibit the diffusion of Cu into solder. The addition of 3 wt.% Sb in the alloy reduces the activation energy of interfacial reaction from 286.41 to 62 kJ/mol, which promotes the interfacial reaction. The addition of 10 wt.% Sb increases the activation energy of interfacial reaction to 686.73 kJ/mol, which inhibits the interfacial reaction and reduces the erosion of the Cu substrate by the solder and inhibits the formation of an excessively thick interfacial layer.

**Key words:** Sn–xSb alloy; interface layer; interface reaction; thermodynamics; solder

### 1 Introduction

Due to the harmful effect of lead on the environment, lead-free solders have been developed and applied in many fields. However, a new solder to replace the Sn–Pb alloy widely used in electronic packaging industry is still under developing due to the poor performance of lead-free solders compared to Sn–Pb alloys in terms of wetting and spreading and joint strength [1,2]. Sb is one of the candidate elements that can be added into the Sn-based alloys instead of Pb [3–6]. Compared with other elements such as Ag or Cu, Sn–Sb alloy is a good substitute for Pb-containing solder because of the good thermal fatigue resistance and high fracture strength [1,7–9]. During the welding process, the wetting behavior and interfacial reaction of solder

greatly influence welding quality and solder joint performance [10–12]. ZENG et al [7] observed a faster reaction rate and a strong dissolution effect at the interface between Sn–Sb alloy and Cu substrate with the increase of Sb content, although the wetting angle did not change much.

The wetting process is usually accompanied by the precipitation of intermetallic compounds (IMCs). Dissolution and chemical reaction have a great influence on the spreading kinetics and the ultimate wettability [13–16]. However, most of the recent studies only focused on the wetting phenomenon, and there was little research on the kinetics of the spreading process. Compared with the wetting behavior of unsaturated and saturated Cu melts on Cu substrate, it was found that the dissolution of the substrate promoted the diffusion of the melt [17]. Similar results have been obtained

from studies about Sn melt on Ag and Ag<sub>3</sub>Sn [18].

Current research on the interface layer between lead-free solder and substrate showed that IMC layers with appropriate thickness and high quality components were beneficial to improving solder joint reliability [19,20]. The research on Sn–3Ag–0.5Cu solder, which has been widely used at present, showed that the interface reaction between Sn-based solder and Cu substrate was severe, and the thick IMC generated by the reaction reduced the reliability of solder joints [21–23]. In addition, the products and properties of interface layer were quite different with different diffusion mechanisms. For example, in Sn/Ni (polycrystalline/single crystal) system, the interface layer formed by Ni atoms provided by grain boundary diffusion in polycrystalline system was Ni<sub>3</sub>Sn<sub>4</sub>, while that provided by lattice diffusion in single crystal system was NiSn<sub>4</sub>, and the corresponding IMC layer was mainly NiSn<sub>4</sub> [24]. Additionally, the properties of Cu<sub>x</sub>Sn<sub>y</sub> IMC layer dominated by temperature gradient were obviously different from those of IMC layer without temperature gradient [25].

From a thermodynamic point of view, the formation of Cu<sub>6</sub>Sn<sub>5</sub> at the interface requires thermodynamic conditions and the diffusion of Cu. Studies of the evolution of IMC layers in Cu/Sn soldering systems have shown that reverse stresses due to non-equilibrium vacancies resulting from imbalances in diffusion fluxes between individual diffusers (Cu and Sn) played a fundamental role in the evolution of IMC layers [26,27]. In a study of hole-to-interface layer growth kinetics, it was found that the Cu/Cu<sub>3</sub>Sn IMC layer can hinder the diffusion of Cu atoms into Sn and promote the generation of the Cu<sub>6</sub>Sn<sub>5</sub> phase [28]. In the study of IMC layers, it was found that the IMC layer with the lowest activation energy formed first and the Cu<sub>6</sub>Sn<sub>5</sub> had higher formation driving force [29]. Besides, the addition of Ag in Sn-based solder promoted the formation of Ag<sub>3</sub>Sn and the morphology of Ag<sub>3</sub>Sn changed from small particles to large flake grains as Ag content increased [30]. The interface reactions occurred between the Ag<sub>3</sub>Sn and Cu<sub>3</sub>Sn IMC layers, which resulted in a large number of Cu<sub>3</sub>Sn particles embedded in the Ag–Sn phase layer and improved the mechanical properties and thermal reliability of the joint. However, the influence of adding elements on the interface layer

was not necessarily monotonous. For example, the Cu<sub>6</sub>Sn<sub>5</sub> IMC layer thickened gradually with the increase of Ni content but became thinner after Ni content exceeded 5 wt.%. On the other hand, the thickness of Cu<sub>3</sub>Sn decreased with increasing Ni content and the number of voids in the Cu<sub>3</sub>Sn layer increased with the thinning of the layer [31].

In conclusion, Sn–Sb alloy is one of the alternatives for the high-temperature lead-free solder. Existing studies have shown that the alloys with a small amount of Sb element still had good wettability and mechanical properties. However, the interface behavior of Sn–Sb alloys during welding process was less studied. The interface products between solder alloy and substrate were directly related to the reliability of solder joint research. In this work, the interface reactions and thermodynamics between Sn–*x*Sb alloys and Cu substrate were studied. The effect of adding Sb on solder joint quality was analyzed from the perspective of reaction kinetics.

## 2 Experimental

### 2.1 Materials preparation

The alloy samples were prepared by mixing Sn powder of 99.99% purity and Sn–10wt.%Sb powder. The powdery mixture was melted in a WK-II-type multifunctional medium frequency induction furnace and then cast into a cylinder with a diameter of 5.5 mm. Alloys with different contents of Sb (0, 0.5, 3.0, 5.0 and 10.0 in wt.%) were prepared. To ensure a uniform composition, the samples were melted at least three times. The cylinder sample was cut into small pieces with a height of 5.5 mm. Oxygen-free Cu plates (15 mm × 15 mm) were used as the substrate. Sandpaper was used to remove surface dirt and oxide layer of the Sn–Sb alloy samples (the Sn–*x*Sb alloys were polished into a  $\varnothing$ 5 mm × 5 mm cylinder) and the Cu substrates before the wetting experiment.

### 2.2 High-temperature wetting experiment

The wetting experiments between Sn–Sb alloy samples and Cu substrate were carried out in the three-phase interface measurement device using the base drop method [32,33]. The Sn–Sb alloy samples were placed on the Cu substrate and kept horizontal. To observe the reaction at the interface

layer, the samples were heated to 873 K with a heating rate of 10 K/min to spread the solder on the Cu substrate and observe the appearance of its interface layer. Heating curve was shown in Fig. 1. These molten samples after cooling were cut from the center by a wire cutter, sealed in epoxy resin with curing agent, and polished. At last, these samples were eroded with 5 vol.% hydrochloric acid alcohol solution for about 30 s followed by cleaning in distilled water and blow-drying before observation.

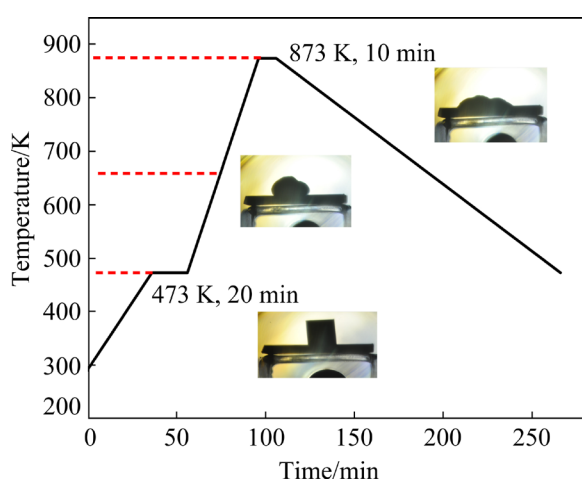


**Fig. 1** Heating curve of high-temperature wetting experiment

The morphology of the interface layer of the samples was observed by SEM and the composition was analyzed by EDS. The effect of Sb on the interfacial reaction was analyzed based on the compositional changes of the interfacial layer.

### 2.3 Thermodynamics of interfacial reaction

A DSA25 differential scanning calorimeter was used to analyze the thermodynamics of interfacial reaction between Sn-*x*Sb alloys and Cu substrate. Two groups of Sn-*x*Sb alloys and Cu discs were placed into a corundum crucible and heated from 298 to 1073 K with the rate of 10 and 15 K/min, respectively. The heating process was taken in Ar atmosphere.

## 3 Results and discussion

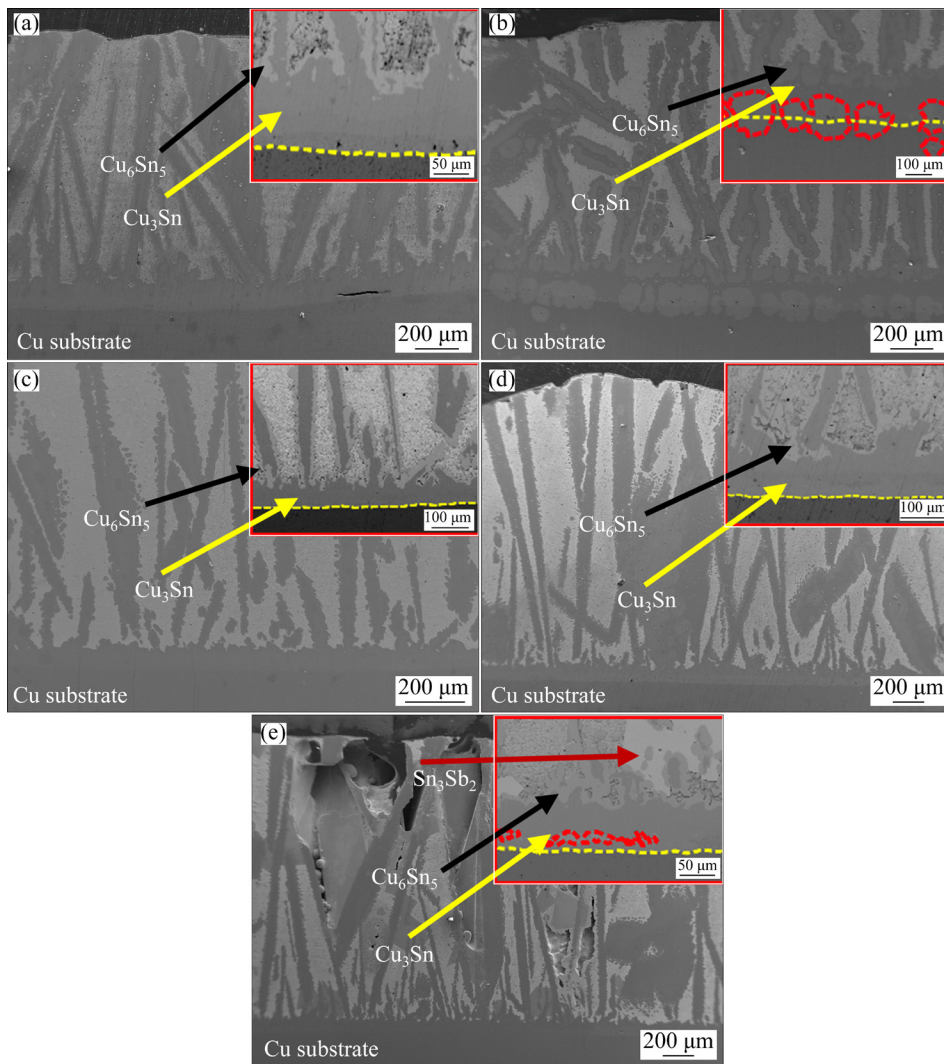
### 3.1 Interface layer morphology

Figure 2 showed the SEM images of the interface between the Sn-*x*Sb alloys with different Sb contents and the Cu substrate at the spreading

stage during wetting. As can be seen, rod-shaped grains gradually grew up in the interface layer after adding Sb. Those rod-shaped grains grew to a certain length and then fell off from the interface layer to the alloy. However, with the increase of Sb content, the distribution of rod-shaped grains at the interface layer showed an increasing-decreasing trend rather than a simple increase or decrease.

During the interfacial reaction between Sn-*x*Sb alloys and Cu substrate, the substrate dissolved into the Sn-*x*Sb alloys and formed the IMC layers. The structure of double or treble interface layer appeared obviously with the rising temperature. The phase in the red-dotted line is  $\text{Cu}_6\text{Sn}_5$ , which appeared at the interface layer when 0.5 wt.% of Sb was added into the alloy. This is because  $\Delta G_{\text{Cu}_3\text{Sn}}$  is more negative than  $\Delta G_{\text{Cu}_6\text{Sn}_5}$  and therefore  $\text{Cu}_6\text{Sn}_5$  is more likely produced first. However, the addition of Sb changed the diffusion rate of Cu and the activation energy of the reaction between Cu and Sn, and the  $\text{Cu}_6\text{Sn}_5$  phase in the red-dotted lines disappeared. While Sb content was 10 wt.%, the  $\text{Cu}_6\text{Sn}_5$  compound layer was formed again. Square particles appeared outside the interface layer, which were  $\text{Sn}_3\text{Sb}_2$  compounds formed by Sb segregation. The segregation of Sb inhibited the diffusion of Cu into the alloy. Cu atoms accumulated at the interface layer and thus formed the  $\text{Cu}_6\text{Sn}_5$  IMC layer near the junction of Cu and  $\text{Cu}_3\text{Sn}$  IMC layer.

Figure 3 showed the cross-section morphology of Sn-*x*Sb alloys after wetting and spreading on Cu substrate. Under the same heating system, the dissolution rate of alloy melt on Cu substrate can be reflected by the dissolution erosion depth, as shown in Table 1. The maximum dissolution erosion depth of Sn-0.5Sb/Cu alloy on Cu substrate was the largest and the interface was the most irregular. The dissolution erosion depth of Sn-10Sb/Cu alloy on Cu substrate was the smallest and the interface was the smoothest. The addition of Sb can inhibit the dissolution of Cu into the alloy and reduce the content of  $\text{Cu}_x\text{Sn}_y$  IMCs in the alloy. It can be seen from Fig. 3 that the left side of the Sn-0.5Sb/Cu alloy interface layer was similar to that of the Sn/Cu interface layer, and the deepest place on the right side of Sn-0.5Sb/Cu alloy interface layer was similar to that of the Sn-*x*Sb/Cu (*x*=5,10) interface layer. It was presumed that less Sb content led to the uneven effect on the erosion process.



**Fig. 2** SEM images of interface between Sn- $x$ Sb alloys with different Sb contents and Cu substrate at spreading stage during wetting (10 K/min, 873 K): (a) Sn; (b) Sn-0.5Sb; (c) Sn-3Sb; (d) Sn-5Sb; (e) Sn-10Sb

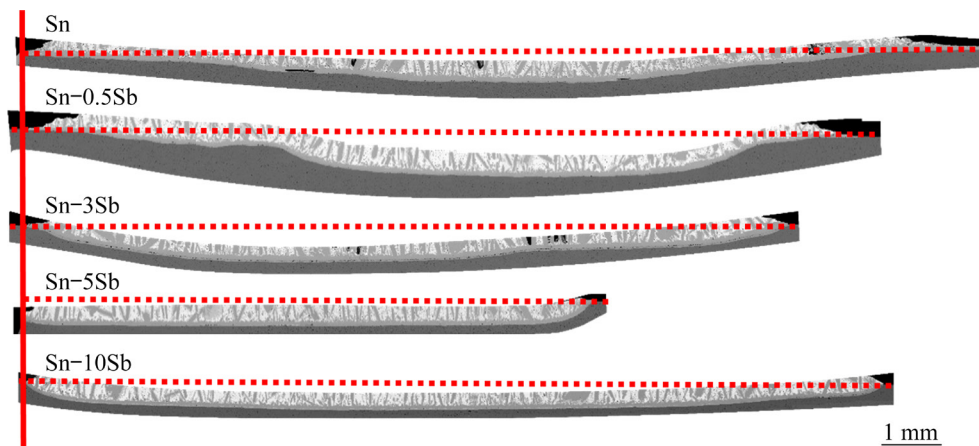


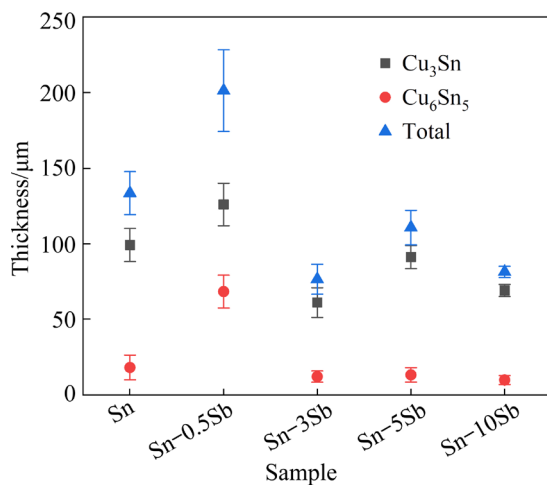
**Fig. 3** Complete morphology comparison of interface layer between spread Sn- $x$ Sb alloy melts and Cu substrate

The thickness of the interfacial layer of the Sn- $x$ Sb alloys after spreading on the Cu substrate was shown in Fig. 4. The interfacial layer was mainly composed of  $\text{Cu}_3\text{Sn}$  layer and  $\text{Cu}_6\text{Sn}_5$  layer.

The thickness of the boundary layer was estimated by measuring 10 sets of different interfacial layer thicknesses for each sample and taking the average value. As can be seen from Fig. 4, the addition of

**Table 1** Dissolution erosion depth of Sn–xSb alloy melts on Cu substrate

Sample	Maximum erosion depth/ $\mu\text{m}$	Average erosion depth/ $\mu\text{m}$
Sn/Cu	644.69	319.65
Sn–0.5Sb/Cu	899.22	455.12
Sn–3Sb/Cu	732.45	525.15
Sn–5Sb/Cu	550.40	488.04
Sn–10Sb/Cu	559.17	378.79

**Fig. 4** Statistics of interface layer thickness with different Sb contents

0.5 wt.% Sb significantly thickened the interfacial layer from 133 to 201  $\mu\text{m}$ , especially the  $\text{Cu}_3\text{Sn}$  layer increased from 99 to 125  $\mu\text{m}$ , which can significantly reduce the reliability of the solder joint due to its brittle nature. While the addition of Sb content was up to 10 wt.%, the thickness of the interfacial side decreased to 81  $\mu\text{m}$  (less than that of pure Sn). Combined with the results of the previous study, it is believed that the  $\text{Sn}_3\text{Sb}_2$  compound formed in the Sn–10Sb alloy precipitates near the interfacial layer, blocking the diffusion channel and producing a shielding effect [30]. It was speculated that the addition of Sb element increased the diffusion energy barriers of elements in the IMC layer, which inhibited the excessive formation of IMC layer and improved the reliability of solder joints.

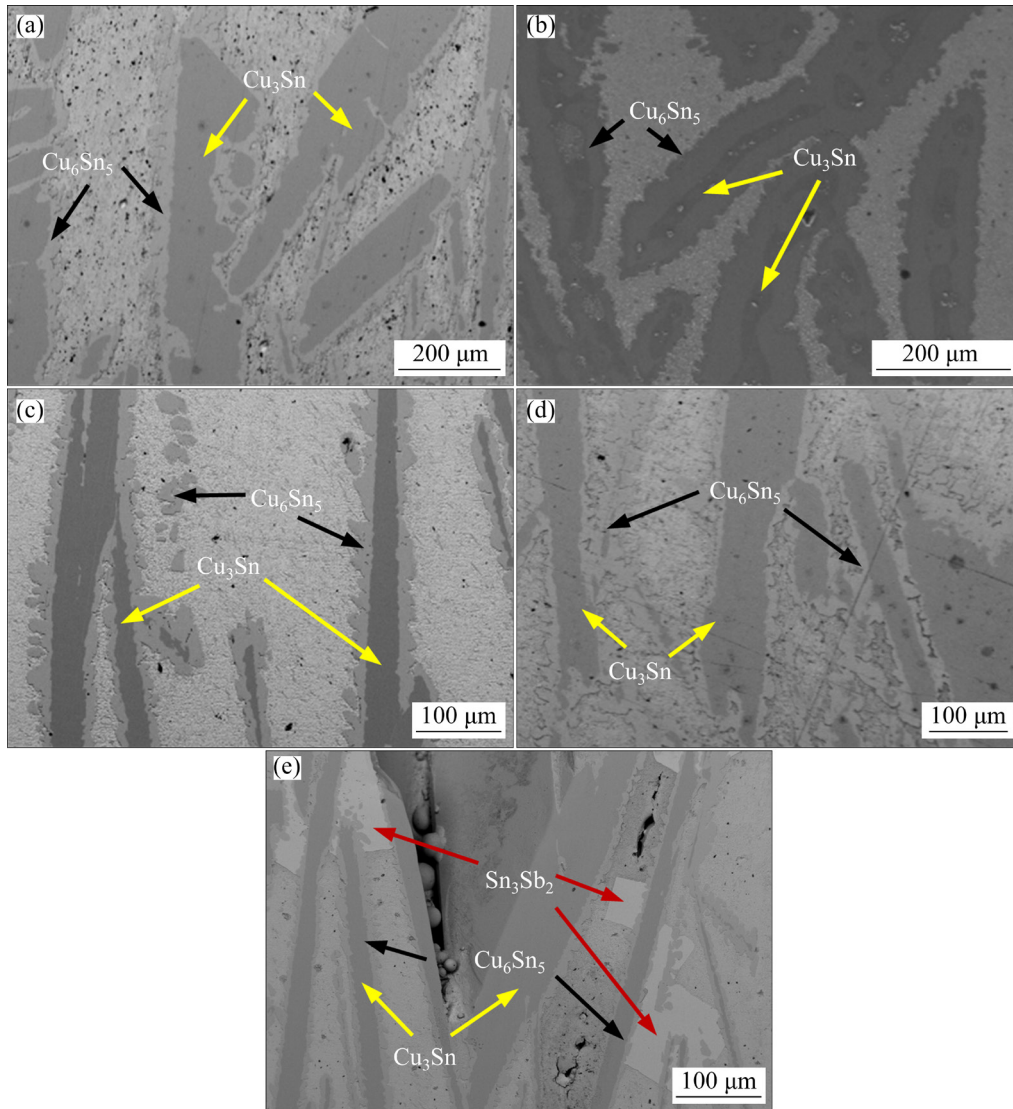
### 3.2 Intermetallic compound in melts

Figure 5 showed the internal microstructure of Sn-based alloys with different Sb contents spread on Cu substrate. The higher temperature improved the spreading of the alloys on the Cu substrate, and

more Cu was dissolved into the alloy to form the rod-like phases. The size of the rod-like phases was dependent on Sb content in the alloys. The rod-like phase became longer and more evenly distributed inside the alloy with the increase of Sb content. These phases were  $\text{Cu}_3\text{Sn}$  in the core surrounded by  $\text{Cu}_6\text{Sn}_5$ . When Sb content was high, as shown in Figs. 5(d, e), some square particles appeared in the alloy, as mentioned above. These particles were  $\text{Sn}_3\text{Sb}_2$  compound according to EDS analysis, which were formed by density segregation of Sb in the alloy. The presence of Sb was not detected in the interface layer or the rod-like structure in the alloy, indicating that Sb did not react with Sn in the alloy or Cu in the substrate. Instead, a tiny concentration gradient of Sb was formed in the alloy as the proceeding of the reaction between Sn and Cu, which caused the segregation of Sb from alloy and aggregation in these small square particles. For the samples in the melting equilibrium stage, the small particles precipitated, the rod-like structures shed off and the heat convection in the heating process became stronger than that in the spreading samples.

The content of Sb influenced the formation of  $\text{Cu}_x\text{Sn}_y$  compounds in the melt. This effect could be characterized by the amount of rod-like structure in the melt. The area proportion of rod-like structure was obtained by Matlab image recognition after binarization processing of SEM images. As shown in Fig. 6, trace addition of Sb contributed to the formation of thick rod-like structure. However, with the increase of Sb content, the generated rod-like structure became longer and thinner compared with the case of pure Sn sample. The rod-like structure with  $\text{Cu}_x\text{Sn}_y$  compound on the cross-section of the alloy melt occupied only 34.69% of the area when Sb content was 10 wt.%. This was because Sb gathered near the interface layer due to segregation, which inhibited the diffusion of Cu into the alloy melt. Cu accumulated at the interface to form  $\text{Cu}_6\text{Sn}_5$ . As shown in Fig. 5(d), the rod-like structure in Sn–5Sb alloy accounted for 51.80% of the area, and there were less  $\text{Cu}_3\text{Sn}$  in the central part and more  $\text{Cu}_6\text{Sn}_5$  in the shell part.

The line in Fig. 6 is the spreading time of alloys. The temperature was around 873 K. The spreading time became longer with increasing Sb content. The spreading time was delayed by 290 s when Sb content increased from 0 to 3 wt.%. When



**Fig. 5** Comparison of rod structure of solder with different Sb contents: (a) Sn/Cu; (b) Sn-0.5Sb/Cu; (c) Sn-3Sb/Cu; (d) Sn-5Sb/Cu; (e) Sn-10Sb/Cu

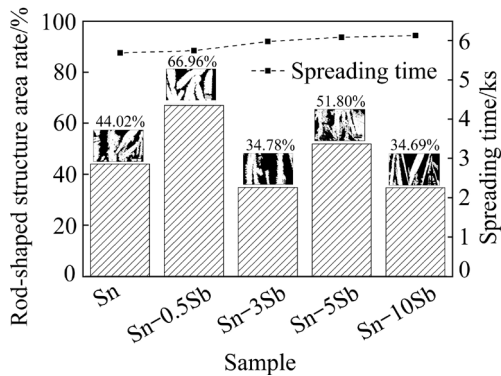


**Fig. 6** Rod-shaped structure area rate and spreading time of samples with different Sb contents

Sb content increased from 3 wt.% to 10 wt.%, the spreading time changed slightly, only 108 s larger. LANDRY and EUSTATHOPOULOS [34] believed

that the spreading of melt was controlled by the formation of new phases, which changed the surface tension between solid and liquid, and provided a driving force for the spreading of melt. In our experiment, the addition of Sb improved the surface tension of the melt. Therefore, the spreading was delayed due to the increased resistance.

### 3.3 Thermodynamics of interfacial reactions

The interfacial reactions between the Sn-xSb alloy and the Cu substrate had a significant influence on the weld quality and welding process parameters. The thermodynamics of the reaction of the Sn-xSb alloy with the Cu substrate was investigated by differential thermal analysis (DTA). Figure 7 showed the DTA curves of the

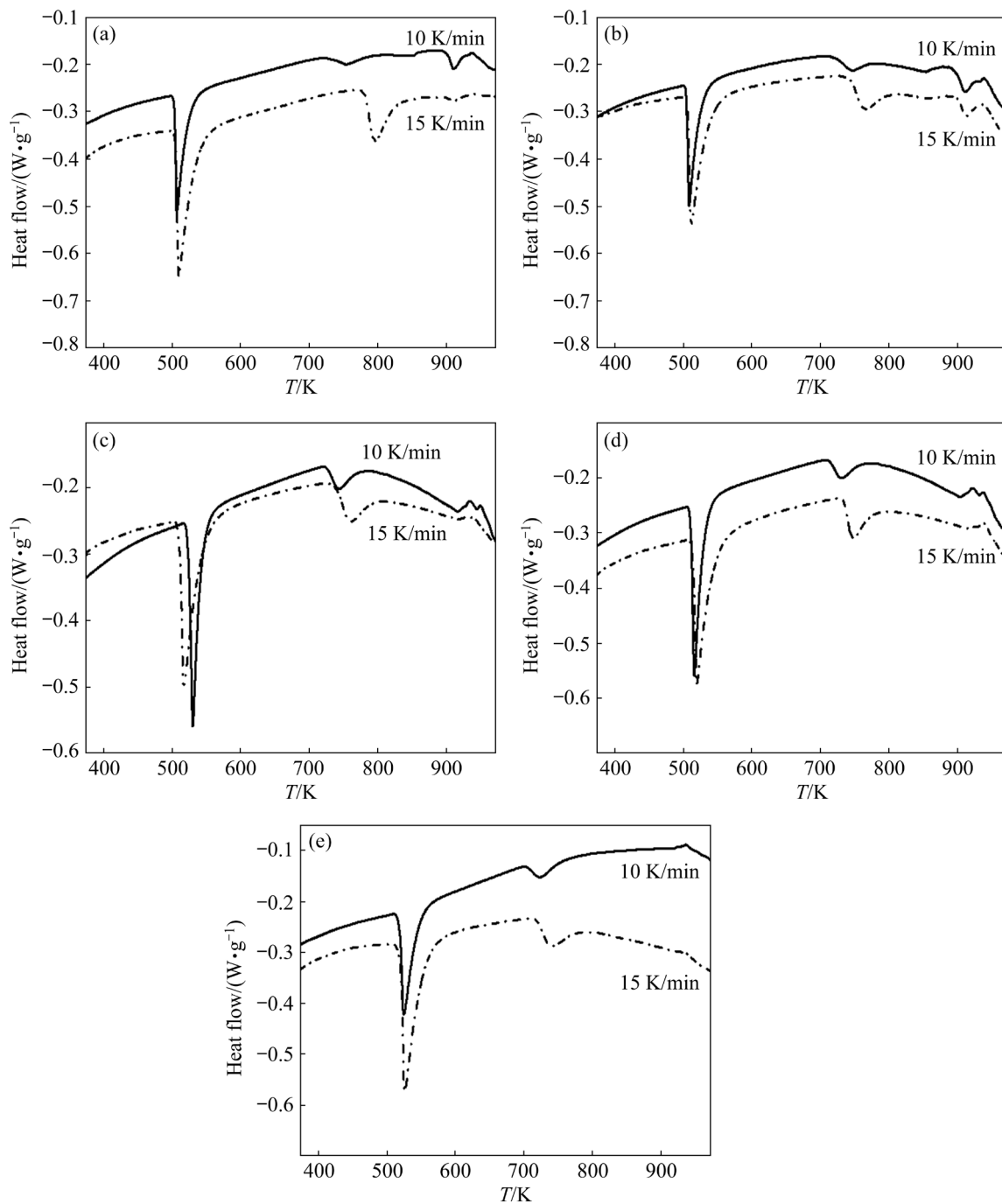


**Fig. 7** DTA curves of reactions between Sn alloy and Cu with different Sb contents: (a) Sn/Cu; (b) Sn-0.5Sb/Cu; (c) Sn-3Sb/Cu; (d) Sn-5Sb/Cu; (e) Sn-10Sb/Cu

Sn- $x$ Sb/Cu system at the temperature rise rates of 10 and 15 K/min, respectively. A strong heat absorption peak appeared around 500 K, containing the melting of the Sn- $x$ Sb alloy and the chemical reaction process of interfacial reactions to form the intermetallic compounds. As the temperature increased, a small heat absorption peak appeared at around 800 K, where further reactions occurred with the further diffusion of Cu atoms into the

interfacial products.

The peak temperature of Sn-3Sb/Cu decreased from 529 to 516 K as the heating rate increased from 10 to 15 K/min (Fig. 7(c)), while the other four samples did not change significantly as the heating rate increased and gradually increased with the increase of the Sb addition.

The thermodynamics of the interfacial reaction was investigated using the Kissinger method [35,36].

The kinetic equations for the system were as follows:

$$\frac{d\eta}{dt} = k_n (1-\eta)^n \quad (1)$$

$$k_n = A \exp[-E_a/(RT)] \quad (2)$$

where  $\eta$  is the reaction conversion rate;  $k_n$  is the reaction rate constant;  $t$  is the reaction time;  $n$  is the order of reaction;  $A$  is the preexponential factor;  $R$  is the molar gas constant;  $T$  is the thermodynamic temperature;  $E_a$  is the reaction activation energy.

According to the Kissinger equation:

$$\frac{d[\ln(\beta/T_m^2)]}{d(1/T_m)} = -\frac{E_a}{R} \quad (3)$$

where  $\beta$  is the heating rate and  $T_m$  is the peak temperature.

The order of reaction  $n$  is

$$n = 1.26\xi^{1/2} \quad (4)$$

where  $\xi$  is the peak shape index.

The thermodynamic parameters calculated from the above equations and the DTA data were shown in Table 2. The effect of the addition of Sb on the interfacial reaction free energy of the system was non-monotone. With the addition of small amount of Sb, the interfacial reaction activation energy first decreased and then increased. The activation energy of the reaction decreased from 286.41 to 62.00 kJ/mol at 3 wt.% Sb addition, but increased to 686.73 kJ/mol at 10 wt.% Sb addition.

The order of reaction of Sn–0.5Sb/Cu was 1.92 and that of Sn–3Sb/Cu was 2.14. This was due to the fact that the process was accompanied by multiple processes of melting, dissolution, chemical reaction and diffusion. While the increase of Sb content reduced the reaction activation energy, the dissolution and diffusion processes did not receive a similar multiplicative increase. The interfacial layer of the Sn–3Sb/Cu system was therefore thinner than that of the Sn–0.5Sb/Cu system (as shown in Fig. 4).

**Table 2** Comparison of thermodynamics parameters of interfacial reaction of Sn– $x$ Sb/Cu

Sample	$E_a/(\text{kJ}\cdot\text{mol}^{-1})$	$A/\text{s}^{-1}$	$n$	$k_n/\text{s}^{-1}$
Sn/Cu	286.41	1.83	2.12	$5.54\times 10^{-30}$
Sn–0.5Sb/Cu	251.96	1.60	1.92	$2.02\times 10^{-26}$
Sn–3Sb/Cu	62.00	0.38	2.14	$2.07\times 10^{-7}$
Sn–5Sb/Cu	234.85	1.45	1.72	$2.43\times 10^{-24}$
Sn–10Sb/Cu	686.73	4.12	1.64	$1.72\times 10^{-68}$

Figure 8 showed the changes of the interfacial layer after natural aging treatment at room temperature for 180 d. The comparison revealed a diffuse distribution of dark grey particles in the interfacial layer of the Sn–3Sb/Cu samples, which were uniformly distributed in the interfacial layer close to the Cu substrate side. Figure 9 showed the results of the mapping analysis of these dark grey

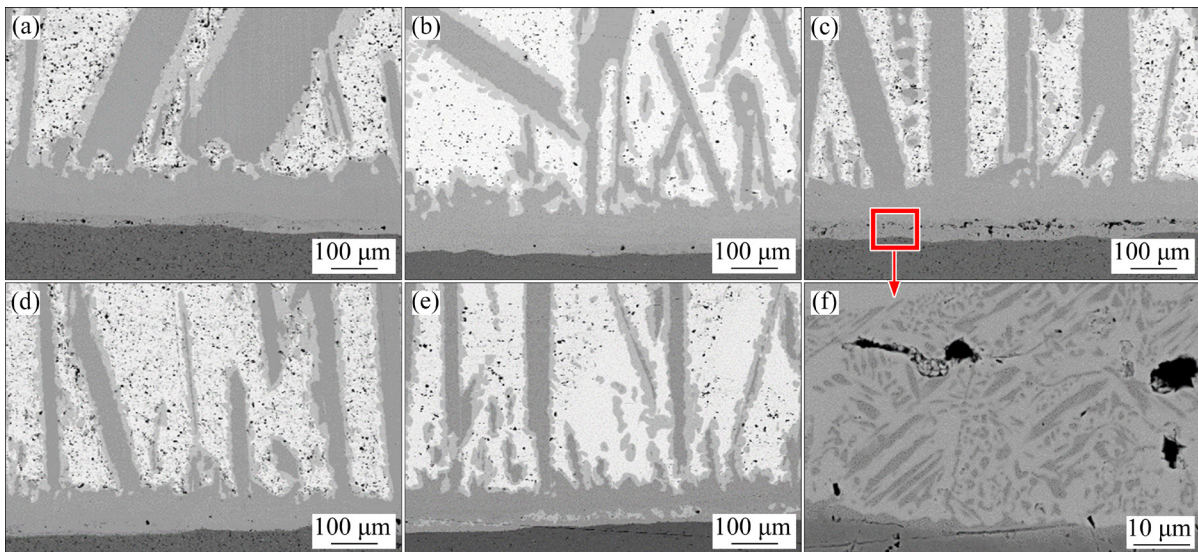


**Fig. 8** Microscopic morphologies of interface layer after nature aging treatment at room temperature for 180 d: (a) Sn/Cu; (b) Sn–0.5Sb/Cu; (c) Sn–3Sb/Cu; (d) Sn–5Sb/Cu; (e) Sn–10Sb/Cu; (f) Particles dispersed in interface layer of Sn–3Sb/Cu

particles using EPMA. The molar ratio of Cu to Sn in these dark grey particles was 9.21:1, while the molar ratio in the dark grey IMC layer close to the substrate side was 1.33:1.

During the natural ageing treatment, the slow diffusion and bonding of Cu and Sn atoms still occurred, but the presence of Sb in the alloy changed the activation energy and diffusion coefficient of the interfacial reaction. Sn–3Sb had the lowest free energy for the interfacial reaction with Cu and was the easiest to react with.

As shown in Fig. 10, Cu atoms diffused into the Sn melt to form the interface layer of  $\text{Cu}_x\text{Sn}_y$  compound. The Cu atoms dissolved into the Sn–Sb alloy and reacted near the interface layer as follows:



The Sn–xSb alloy wetted and spread on the Cu substrate and reacted with it after melting. The solid Cu dissolved into the Sn melt while the liquid Sn diffused into the Cu substrate. When Cu saturated near the interface, the IMC layer nucleated and grew on the Cu substrate, formed the  $\text{Cu}_6\text{Sn}_5$  which aggregated at the Cu/ $\text{Cu}_3\text{Sn}$  interface. However,  $\text{Cu}_6\text{Sn}_5$  was not thermodynamically stable and therefore continued to react with the dissolved Cu to form  $\text{Cu}_3\text{Sn}$  during continuous heating, as shown in Fig. 10. The thickness of the interfacial layer was determined by both the rate of atomic expansion

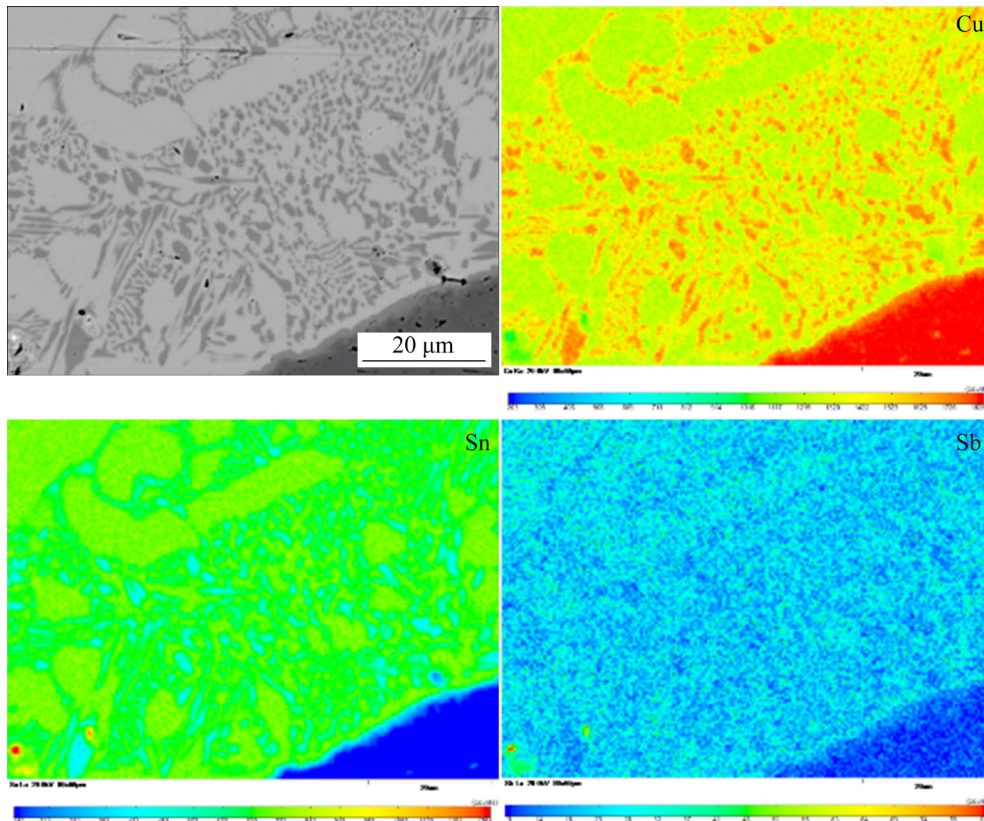


Fig. 9 EPMA mapping results of gray particles in interfacial layer of Sn–3Sb/Cu samples

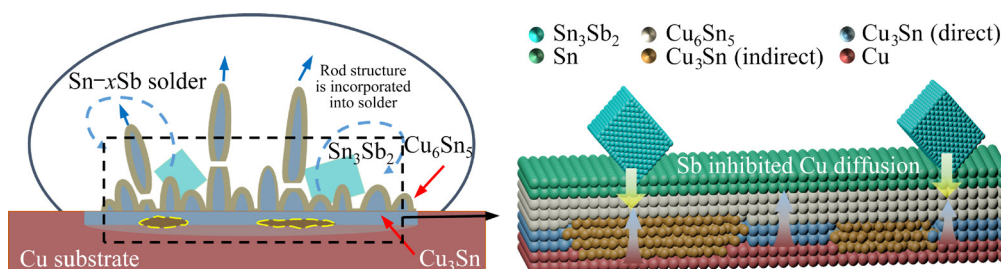


Fig. 10 Illustration of Sn–xSb/Cu interfacial reactions and behavior of intermetallic compounds

and the rate of interfacial reaction. As the reaction progressed, the interfacial products gradually grew into a rod-like structure with an outer layer of  $\text{Cu}_6\text{Sn}_5$  and an inner layer of  $\text{Cu}_3\text{Sn}$ . Due to the thermal convection inside the melt and the brittle nature of the  $\text{Cu}_3\text{Sn}$ , they fell off from the interfacial layer and moved towards the interior of the melt. Due to the concentration gradient and temperature gradient of the materials, the convection currents generated in the melt affect the diffusion rate of the components within the melt. The diffusion rates of the Cu and Sn atoms differed and so did the growth rate of the interfacial layer. The thickness of the interfacial side was determined by the atomic diffusion rate. Bias of Sb inhibited the growth of the interfacial layer, mainly by reducing the diffusion of Sn and Cu.

## 4 Conclusions

(1) Through the analysis of samples after wetting experiment between Sn-based alloys with different Sb contents and a Cu substrate, it was found that when the interfacial reaction attained equilibrium, there may be three interface layers, due to the difference in diffusion rate of elements. The addition of Sb had obvious influence on the diffusion rate of Cu.

(2) With the addition of Sb, the initial reaction time of Sn- $x$ Sb alloy and Cu showed an increase-decrease tendency. The elements in the alloy affected the growth of the interface layer. Sb inhibited Cu diffusion, thus inhibited the formation of the interface layer. However, this effect was only obvious when the content of Sb in the alloy was high.

(3) The  $\text{Cu}_6\text{Sn}_5$  phase formed between Cu and  $\text{Cu}_3\text{Sn}$  layers in the case of Sn-0.5Sb alloy. This is because during the transition from  $\text{Cu}_3\text{Sn}$  layer to  $\text{Cu}_6\text{Sn}_5$  layer, Cu diffusion was inhibited, the reaction rate of  $\text{Cu}_6\text{Sn}_5$  and Cu decreased near the solder. This trend caused the rod to fall off more quickly into the alloy bulk, resulting in more cracks in the interface layer.

(4) The Sb content of less than 10 wt.% promoted the interfacial reaction process, generated a thicker interfacial layer, and reduced the quality of the solder joint. However, when the Sb addition reached 10 wt.%, it reduced the interfacial reaction activity. It inhibited the interfacial reaction process

to reduce the erosion of the Cu substrate and the production of an excessively thick interfacial layer, which improved the quality of the solder joint.

## Acknowledgments

This research work was supported by the National Natural Science Foundation of China (Nos. U1738101, 51974022) and Fundamental Research Funds for the Central Universities, China (No. FRF-MP-20-17).

## References

- [1] KOBAYASHI K, SHOHJI I, KOYAMA S, HOKAZONO H. Fracture behaviors of miniature size specimens of Sn-5Sb lead-free solder under tensile and fatigue conditions [J]. *Procedia Engineering*, 2017, 184: 238–245.
- [2] SUGANUMA K, KIM S J, KIM K S. High-temperature lead-free solders: Properties and possibilities [J]. *JOM*, 2009, 61: 64–71.
- [3] ROCHA O L, COSTA T A, DIAS M, GARCIA A. Cellular/dendritic transition, dendritic growth and microhardness in directionally solidified monophasic Sn-2%Sb alloy [J]. *Transactions of Nonferrous Metals Society of China*, 2018, 28: 1679–1686.
- [4] GERANMAYEH A R, NAYYERI G, MAHMUDI R. Microstructure and impression creep behavior of lead-free Sn-5Sb solder alloy containing Bi and Ag [J]. *Materials Science and Engineering A*, 2012, 547: 110–119.
- [5] ASANTE J K O, TERBLANS J J, ROOS W D. Segregation of Sn and Sb in a ternary Cu(100)SnSb alloy [J]. *Applied Surface Science*, 2005, 252: 1674–1678.
- [6] TAO Q B, BENABOU L, VIVET L, LE V N, OUEZDOU F B. Effect of Ni and Sb additions and testing conditions on the mechanical properties and microstructures of lead-free solder joints [J]. *Materials Science and Engineering A*, 2016, 669: 403–416.
- [7] ZENG Qiu-lian, GUO Jian-jun, GU Xiao-long, ZHAO Xin-bing, LIU Xiao-gang. Wetting behaviors and interfacial reaction between Sn-10Sb-5Cu high temperature lead-free solder and Cu substrate [J]. *Journal of Materials Science and Technology*, 2010, 26: 156–162.
- [8] EL-DALY A A, SWILEM Y, HAMMAD A E. Creep properties of Sn-Sb based lead-free solder alloys [J]. *Journal of Alloys and Compounds*, 2009, 471: 98–104.
- [9] CHIDAMBARAM V, HATTEL J, HALD J. High-temperature lead-free solder alternatives [J]. *Microelectronic Engineering*, 2011, 88: 981–989.
- [10] DIAS M, COSTA T A, SILVA B L, SPINELLI J E, CHEUNG N, GARCIA A. A comparative analysis of microstructural features, tensile properties and wettability of hypoperitectic and peritectic Sn-Sb solder alloys [J]. *Microelectronics Reliability*, 2018, 81: 150–158.
- [11] DIAS M, COSTA T, ROCHA O, SPINELLI J E, CHEUNG

- N, GARCIA A. Interconnection of thermal parameters, microstructure and mechanical properties in directionally solidified Sn–Sb lead-free solder alloys [J]. *Materials Characterization*, 2015, 106: 52–61.
- [12] ZHANG Cheng, LIU Si-dong, QIAN Guo-tong, ZHOU Jian, XUE Feng. Effect of Sb content on properties of Sn–Bi solders [J]. *Transactions of Nonferrous Metals Society of China*, 2014, 24: 184–191.
- [13] WEBB E B, GREY G S, HEINE D R, HOYT J J. Dissolutive wetting of Ag on Cu: A molecular dynamics simulation study [J]. *Acta Materialia*, 2005, 53: 3163–3177.
- [14] LIN Qiao-li, JIN Peng, CAO Rui, CHEN Jian-hong. Reactive wetting of low carbon steel by Al 4043 and 6061 alloys at 600–750 °C [J]. *Surface and Coatings Technology*, 2016, 302: 166–172.
- [15] YIN Liang, MURRAY B T, SINGLER T J. Dissolutive wetting in the Bi–Sn system [J]. *Acta Materialia*, 2006, 54: 3561–3574.
- [16] YIN Liang, MESCHTER S J, SINGLER T J. Wetting in the Au–Sn system [J]. *Acta Materialia*, 2004, 52: 2873–2888.
- [17] PROTSENKO P, GARANDET J P, VOYTOVYCH R, EUSTATHOPOULOS N. Thermodynamics and kinetics of dissolutive wetting of Si by liquid Cu [J]. *Acta Materialia*, 2010, 58: 6565–6574.
- [18] LIASHENKO O Y, HODAJ F. Wetting and spreading kinetics of liquid Sn on Ag and Ag<sub>3</sub>Sn substrates [J]. *Scripta Materialia*, 2017, 127: 24–28.
- [19] ZHANG Zhe, HU Xiao-wu, JIANG Xiong-xin, LI Yu-long. Influences of mono-Ni(P) and dual-Cu/Ni(P) plating on the interfacial microstructure evolution of solder joints [J]. *Metallurgical and Materials Transactions A*, 2019, 50(1): 480–492.
- [20] HAN Yong-dian, YANG Jia-hang, XU Lian-yong, JING Hong-yong, ZHAO Lei. Effect of transient current bonding on interfacial reaction in Ag-coated graphene Sn–Ag–Cu composite solder joints [J]. *Transactions of Nonferrous Metals Society of China*, 2021, 31(8): 2454–2467.
- [21] WANG Hao-zhong, HU Xiao-wu, JIANG Xiong-xin. Effects of Ni modified MWCNTs on the microstructural evolution and shear strength of Sn–3.0Ag–0.5Cu composite solder joints [J]. *Materials Characterization*, 2020, 163: 110287.
- [22] WANG Hao-zhong, HU Xiao-wu, JIANG Xiong-xin, LI Yu-long. Interfacial reaction and shear strength of ultrasonically-assisted Sn–Ag–Cu solder joint using composite flux [J]. *Journal of Manufacturing Processes*, 2021, 62: 291–301.
- [23] BI Xiao-yang, HU Xiao-wu, LI Qing-lin. Effect of Co addition into Ni film on shear strength of solder/Ni/Cu system: Experimental and theoretical investigations [J]. *Materials Science and Engineering A*, 2020, 788: 139589.
- [24] WANG Jia-ning, CHEN Jie-shi, ZHANG Zhi-yuan, ZHANG Pei-lei, YU Zhi-shui, ZHANG Shu-ye. Effects of doping trace Ni element on interfacial behavior of Sn/Ni (polycrystal/single-crystal) joints [J]. *Soldering & Surface Mount Technology*, 2021, 34(2): 124–133.
- [25] QIAO Yuan-yuan, MA Hai-tao, YU Feng-yun, ZHAO Ning. Quasi-in-situ observation on diffusion anisotropy dominated asymmetrical growth of Cu–Sn IMCs under temperature gradient [J]. *Acta Materialia*, 2021, 217: 117168.
- [26] SOBIECH M, KRÜGER C, WELZEL U, WANG Jiang-yang, MITTEMEIJER E J, HÜGEL W. Phase formation at the Sn/Cu interface during room temperature aging: Microstructural evolution, whiskering, and interface thermodynamics [J]. *Journal of Materials Research*, 2011, 26(12): 1482–1493.
- [27] SHAO Hua-kai, WU Ai-ping, BAO Yu-dian, ZHAO Yue, ZOU Gui-sheng, LIU Lei. Microstructure evolution and mechanical properties of Cu/Sn/Ag TLP-bonded joint during thermal aging [J]. *Materials Characterization*, 2018, 144: 469–478.
- [28] ROSS G, VUORINEN V, PAULASTO-KRÖCKEL M. Void formation and its impact on CuSn intermetallic compound formation [J]. *Journal of Alloys and Compounds*, 2016, 677: 127–138.
- [29] CHOI W K, LEE H M. Prediction of primary intermetallic compound formation during interfacial reaction between Sn-based solder and Ni substrate [J]. *Scripta Materialia*, 2002, 46(11): 777–781.
- [30] TUNTHAWIROON P, KANLAYASIRI K. Effects of Ag contents in Sn–xAg lead-free solders on microstructure, corrosion behavior and interfacial reaction with Cu substrate [J]. *Transactions of Nonferrous Metals Society of China*, 2019, 29(8): 1696–1704.
- [31] VUORINEN V, LAURILA T, MATTILA T, HEIKINHEIMO E, KIVILAHTI J K. Solid-state reactions between Cu(Ni) alloys and Sn [J]. *Journal of Electronic Materials*, 2007, 36(10): 1355–1362.
- [32] YUAN Zhang-fu, MUKAI K, TAKAGI K, OHTAKA M, HUANG Wen-lai, LIU Qiu-sheng. Surface tension and its temperature coefficient of molten tin determined with the sessile drop method at different oxygen partial pressures [J]. *Journal of Colloid and Interface Science*, 2002, 254(2): 338–345.
- [33] YUAN Zhang-fu, WANG Rong-yue, YU Xiang-tao. Marangoni-convection-driven bubble behavior and microstructural evolution of Sn–3.5Ag/Sn–17Bi–0.5Cu (wt pct) alloy solidified on Cu substrate under space microgravity condition [J]. *Metallurgical and Materials Transactions A*, 2019, 50(11): 5210–5220.
- [34] LANDRY K, EUSTATHOPOULOS N. Dynamics of wetting in reactive metal/ceramic systems: Linear spreading [J]. *Acta Materialia*, 1996, 44: 3923–3932.
- [35] BLAINE R L, KISSINGER H E. Homer Kissinger and the Kissinger equation [J]. *Thermochimica Acta*, 2012, 540: 1–6.
- [36] XU Hong-yan, YUAN Zhang-fu. Interfacial reaction kinetics between liquid Sn–Ag–Cu alloys and Cu substrate [J]. *Rare Metal Materials and Engineering*, 2014, 43(12): 2893–2897.

# Sn-xSb 合金与 Cu 基体的界面反应行为及热力学

王容岳<sup>1</sup>, 袁幸福<sup>1</sup>, 赵宏欣<sup>2</sup>, 杨肖<sup>3</sup>, 郝煜辉<sup>1</sup>

1. 北京科技大学 钢铁共性技术协同创新中心, 北京 100083;

2. 中国科学院 过程工程研究所, 北京 100190;

3. 西湖大学 工学院, 杭州 310024

**摘要:** 研究不同 Sb 含量 Sn-Sb 合金在 Cu 基板上的界面行为, 以明确 Sb 元素对 Sn-Sb 合金焊料焊接可靠性的影响。通过分析 Sn-xSb/Cu 体系的显微组织和界面反应热力学, 解释界面层的演化过程。结果表明, 添加 Sb 对金属间化合物层的生长并非单调递增。Sb 能抑制 Cu 在焊料中的扩散。添加 3% Sb (质量分数)使界面反应活化能从 286.41 降低到 62 kJ/mol, 促进了界面反应的进行。随着 Sb 含量增加至 10% Sb (质量分数), 界面反应活化能提高到 686.73 kJ/mol, 使界面反应难度增加, 减少焊料对 Cu 基体的熔蚀, 并抑制过厚界面层的形成。

**关键词:** Sn-xSb 合金; 界面层; 界面反应; 热力学; 焊料

(Edited by Wei-ping CHEN)